# Supplementary Information for

# Organism motility in an oxygenated shallow-marine environment 2.1 billion years ago

Abderrazak El Albani[a,1*], M. Gabriela Mangano[b], Luis A. Buatois[b], Stefan Bengtson[c], Armelle Riboulleau[d], Andrey Bekker[e], Kurt Konhauser[f], Timothy Lyons[e], Claire Rollion-Bard[g], Olabode Bankole[a], Stellina Gwenaelle Lekele Baghekema[a], Alain Meunier[a], Alain Trentesaux[d], Arnaud Mazurier[a], Jeremie Aubineau[a], Claude Laforest[a], Claude Fontaine[a], Philippe Recourt[d], Ernest Chi Fru[h], Roberto Macchiarelli[i,j], Jean Yves Reynaud[d], François Gauthier-Lafaye[k], Donald E. Canfield[l*].


[a]UMR CNRS IC2MP 7285, University of Poitiers, 86073 Poitiers, France. [b] Department of Geological Sciences, University of Saskatchewan, Saskatoon, SK S7N 5A5, Canada. [c]Department of Palaeobiology, Swedish Museum of Natural History, Box 50007, SE-104 05 Stockholm, Sweden. [d]UMR 8187 LOG CNRS, University of Lille, ULCO, 59655, Villeneuve d'Ascq, France. [e]Department of Earth Sciences, University of California, Riverside, California 92521, USA. [f]Department of Earth and Atmospheric Sciences University of Alberta Edmonton, Alberta, T6G 2E3 Canada. [g]Institut de Physique du Globe de Paris, Sorbonne Paris Cité, Université Paris Diderot, UMR 7154 CNRS, F-75005 Paris, France. [h]Cardiff University, Main Building, Room 2.15B Park Place Cardiff, CF10 3AT, UK. [i]Unité de Formation Géosciences, Université de Poitiers, 86073 Poitiers, France. [j]UMR 7194 CNRS, Muséum National d'Histoire Naturelle, Paris, France. [k]Laboratoire d'Hydrologie et de Géochimie de Strasbourg, UMR 7517 CNRS, 67084, Université de Strasbourg, France. [l]Nordic Center for Earth Evolution, DK-5230 Odense M, Denmark.


*Corresponding author: Donald E. Canfield (Dec@biology.sdu.dk)

*Co-corresponding author: A. El Albani (abder.albani@univ-poitiers.fr),

This PDF file includes:

Supplementary texts 1, 2 and 3
Figs. S1 to S12
Videos S1 to S5
Tables S1 to S2
References for SI reference citations

## Supplementary Information Text 1
## Microbially induced sedimentary structures

Microbially induced sedimentary structures (MISS) of the Francevillian Series have been recently discussed in detail (1). In addition, Figure S3 shows six representative types of exceptionally well-preserved MISS comprising elephant-skin textures, domal buildups, nodular structures, wrinkle structures and Kinneyia structures from the FB2 Member. The wide variability of MISS and the close association with the string-shaped structures might imply that cyanobacteria communities on the one hand produced benthic $O_2$ oases and, on the other hand, facilitated the pre-lithification processes in the sediment.

The fairy-ring structures (Fig. S3A) correspond to a specific group of discoidally shaped microbial colonies and are found on a single bedding plane of silty black shales. The ring-shaped structure is defined by pyritized concentric bands with series of light and dark zones about 4 mm wide. The invoked mechanism for the origin of this MISS is concentric wave propagation triggered by escape of gas bubbles, in which filamentous cyanobacteria controlled by chemotactic responses colonized the bedding plane (2, 3).

Thin biofilm layers described as wrinkle structures were observed on the upper surface of sandstones (Fig. S3B). The surface is marked by well-defined sinuous and continuous ridges and valleys. The sub-parallel ridges display rounded tops and steep sides 3–4 mm wide, 1 mm high; the intercrest space is about 4 mm. Previous studies have proposed numerous interpretations about the process of the formation of wrinkle structures (4–8). Recently, in a wave-tank experiment, (9) reproduced small-scale wrinkle structures by means of microbial aggregates rolling along the substrate and transporting grains.

The Kinneyia structures were found on bedding plane of silty black shales (Figs. S3C, D). They are characterized by distinct short, sinuous, flat-topped ridges, 1 mm high and 2 mm wide, separated by parallel troughs. Kinneyia structures are one of the most common and problematic MISS (10) from its initial description as fossil algae (11) until the present day, when the term is used for a group of mat-related structures. They have been interpreted in different ways - as structures formed beneath the mat layers (e.g., 6, 8, 10, 11) or as biologically mediated structures generated at the water-sediment interface (9).

The horizontal mat growth pattern (Fig. S3E) could be related to fairy-ring structures, in which ridges share some similarities (*e.g.,* sharp-crested, organized). This morphology may result from the same process that is responsible for the fairy-ring formation with added

topography. By secreting extracellular polymeric substances, microbial mats become a viscoelastic, firm film (13). Under these conditions, wave propagation might generate millimeter-scale ripples. Pinnacle-forming organisms would then respond to nutrient gradient via chemotaxis, biostabilizing the substrate. However, the horizontal mat growth pattern could also be merely the result of the substrate topography without any stimulus influence. In this case, the microbial carpet would gently spread, propagating substrate topography upward. The parallel arrangement of ridges and the regularity of components in the horizontal mat growth pattern suggest its biotic origin.

Domal buildups (Fig. S3F) are preserved as clustered, low mound-shaped structures, ~4 mm in diameter on bedding plane of silty black shales. They are also pyritized and protrude about a millimeter above the surface. Circular disks of the Francevillian large colonial organisms (14) are occasionally associated with these structures. Flat, pyritized mat-related structures could also grade into featureless bedding planes. Previous studies have suggested that domal structures are caused by an upward growth of microbial mats and thus might reflect competition for light (15, 16).

Elephant-skin textures (Figs. S3G-H, (17)) are characterized by millimeter to centimeter-size ridges or bulges forming a distinct reticulate texture on upper surface of fine- to coarse-grained sandstones. The maximum relief of this network is 2 mm. This structure might be produced by a vertical growth of cyanobacteria in response to phototaxis (18). However, (19) suggested that it might be related to an undirected gliding of filamentous cyanobacteria merely influenced by their own morphotype.

**Supplementary Information Text 2**

**Comparison of Francevillian string-shaped structures with synaeresis cracks and pyrite precipitation associated with fluid migration**

Synaeresis cracks typically develop in low-energy environments where shales or mudstones are interbedded with fine-grained sandstones or siltstones. They may curve sharply and can be dilated by compression (Fig. S10); synaeresis cracks filled with sand or silt differ in compaction style from the adjacent sediments (20, 21). Synaeresis cracks take on a variety of morphologies (Fig. S10), all of which result from the different degree of deformation of initial fractures that were originally planar (20, 22). For this reason, they can be easily distinguished from vermiform trace fossils and tubular objects (Table S2). The occasional oblique-to-the-bedding orientation of the Francevillian string-shaped structures might seem similar to water-escape structures guided by synaeresis cracks (Fig. S10). However, pyritization of these structures and their shapes and dimensions, whether they are horizontal or oblique, are inconsistent with formation through sediment displacement by fluidization (Table S2).

Pyrite precipitation associated with fluid migration is controlled by two main processes. One is linked to subsurface hydrothermal fluid circulation. Typical examples of such precipitates are sedimentary exhalative ore deposits (SEDEX), where galena and sphalerite are dominant ores, but pyrite and sometimes barite are also abundant. SEDEX mineralisation is dominantly stratiform (23, 24). The Francevillian Basin compartmentalized by major synsedimentary faults (25) could represent a favourable context for the origin of SEDEX ore deposits. While the Francevillian pyritized string-shaped structures do not represent morphologies typical for SEDEX ore deposits, the bedding-parallel pyritic bacterial mats might show resemblance with stratiform SEDEX mineralisation (24). Nevertheless, galena, sphalerite and barite are largely absent from the FB2 Member. Furthermore, $\delta^{34}$S values of pyrite in SEDEX deposits are typically positive (23, 26) and markedly different from the values measured for the Francevillian string-shaped structures.

The second possible setting for pyrite precipitations is that associated with vents where high-temperature hydrothermal fluids emanate. However, this setting produces the same mineral association as SEDEX deposits (27, 28) and for this reason cannot account for the Francevillian string-shaped structures. Mineral precipitates associated with cold seeps and methane vents are dominated by carbonates, but pyrite is also frequently observed as a by-product of the anaerobic oxidation of methane (29). In particular, pyrite often replaces or fills

shells of organisms living in proximity to methane seeps (e.g., 29). In cold vents and methane seeps, pyrite also forms tubular structures whose diameter varies from several centimetres for chimneys (31) to less than 1 millimetre (30). These tubular structures are generally vertically oriented, parallel to fluid escape, and pyrite has different habitus: anhedral, euhedral, coliform and framboidal (29). Considering that the Francevillian string-shaped structures are predominantly developed on the bedding plane and are not associated with other mineral precipitates common in cold seeps and methane vents such as carbonates with highly negative C isotope values and barites with highly positive S isotope values, it seems very unlikely that the Francevillian string-shaped structures developed in these environments.

**Supplementary Information Text 3**

**Comparison of Francevillian string-shaped structures with co-occurring network of interconnected rings**

String-shaped structures in the Francevillian FB2 Member could be confused with the network of interconnected rings (previously described by (14, 32)), which are also developed along the bedding plane and have walls made of thin pyritic strands (Fig. S11). The rings are mostly circular and about 2–5 cm in diameter. The strings connected to the rings are either open-ended (Fig. S11E, bottom center) or closed in a loop containing several rings (Fig. S11E, upper center), suggesting that at least some of them may have been a component of more complex ring (Fig. S11F, lower part). At three-string junctions (as when a free string attached to a ring) the strings widen to produce a triangular plate (Figs. S11B–E). Although the strings can generally be followed as pyritized strands, parts of the strings are divided into more-or-less regularly spaced globular pyrite aggregates (Fig. S11E).

The network of interconnected rings might be biogenic structure, somewhat resembling the Ediacaran body fossil *Palaeopascichnus*, originally interpreted as a meandering trace fossil (33). Short fragments missing the branching points may be mistaken for simpler varieties of the string-shaped fossils that are the focus of this paper; we have not observed network sections with sinuous-contorted shape or traversing the shale laminations at steep angles such as in the string-shaped structures. In any case, the morphology of the network of interconnected rings is not compatible with the mode of formation of the string-shaped structures as interpreted in this study, and thus the two are not likely to be genetically related.
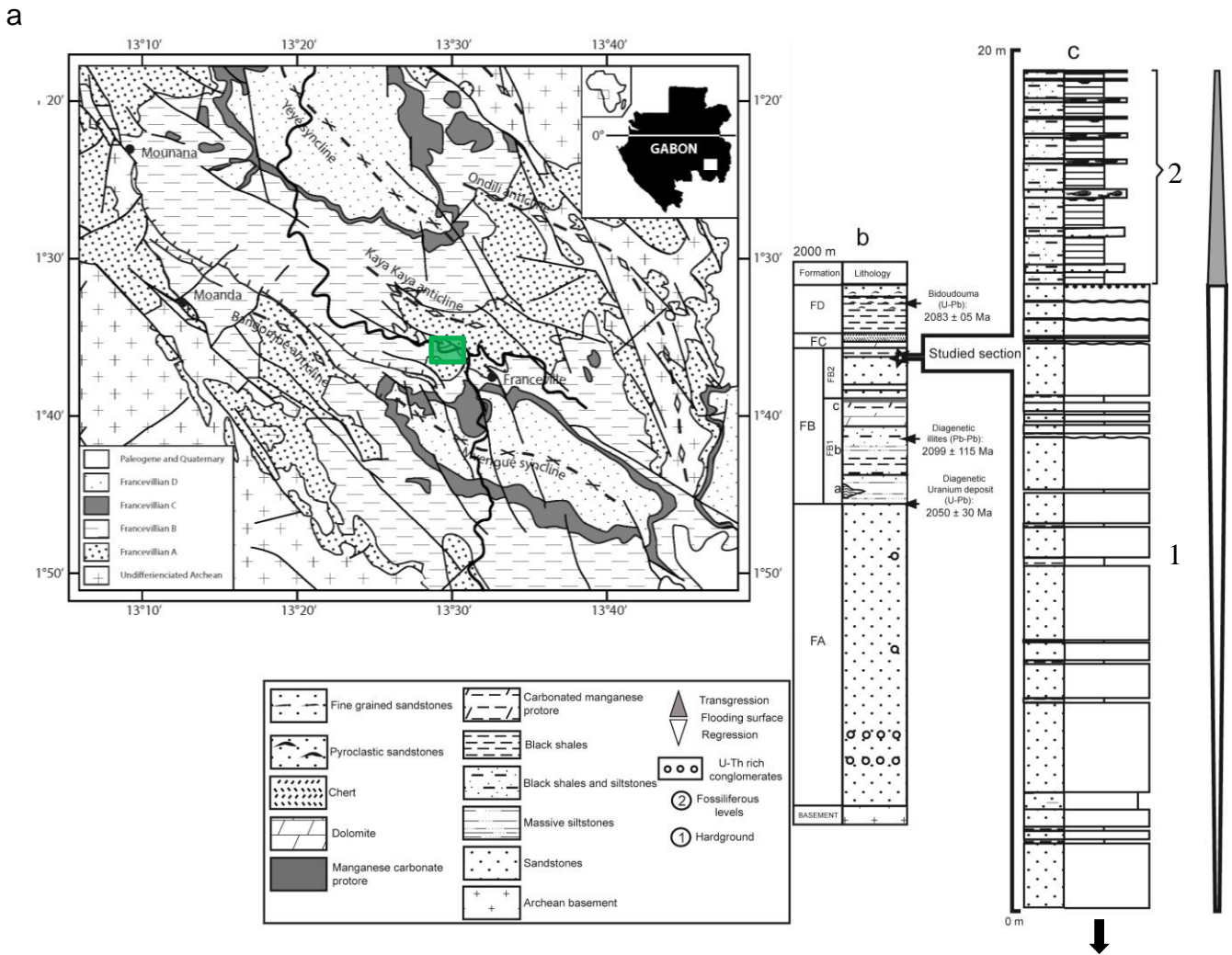
**Fig. S1.** (A) Geological map of the Francevillian basin and location of the studied area (green rectangle). (B) Lithostratigraphy of the Paleoproterozoic Francevillian Series that consists of four formations (FA to FD). The lower part of the FB2 Member consists of sandstone beds deposited above the fair-weather wave base representing a prograding shoreline. (C) The upper part of the FB2 Member (the FB2b unit, black star on b) conformably sits on an oxidized, hardground surface. It consists of a 5 m-thick deposit of finely laminated black shales bearing the string-shaped structures and interbedded with thin silty sandstone layers. String-shaped structures are most abundant in the basal meter of the section while the previously described macrofossils (14, 32) are distributed throughout the 5 meter-thick section of black shales. The age of the FB Formation is constrained to 2100 ± 30 Ma (14, 32). Black arrow at the bottom of the schematic section indicates the further extension of the FA Formation for 1000 m.
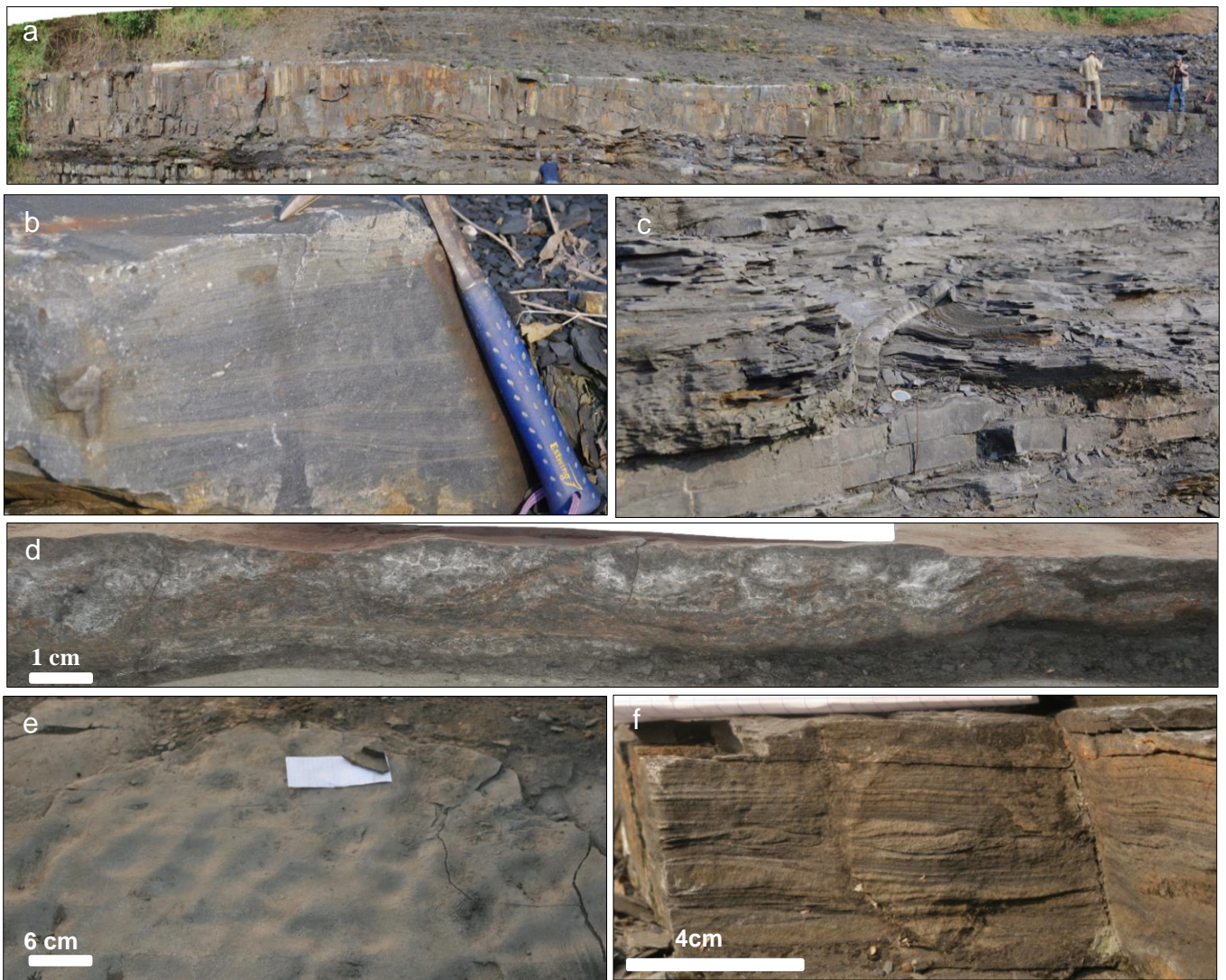
**Fig. S2.** Panoramic view and field photographs of sedimentary facies at the Moulendé Quarry (transition of the FB2a to FB2b unit). (A) Transition from massive sandstone to thinly-laminated silty black shales. (B) Cross-sectional view of decimeter-scale hummocky cross-stratification from massive sandstone. (C) Sandstone dyke at the transition between sandstone and silty black shales. Coin diameter is ~2 cm. (D) Cross-sectional view of convoluted bedding within the intercalated siltstone. (E) Bedding plane view of interference ripples from the upper part of the sequence. (F) Cross-sectional view of current ripples in siltstone.
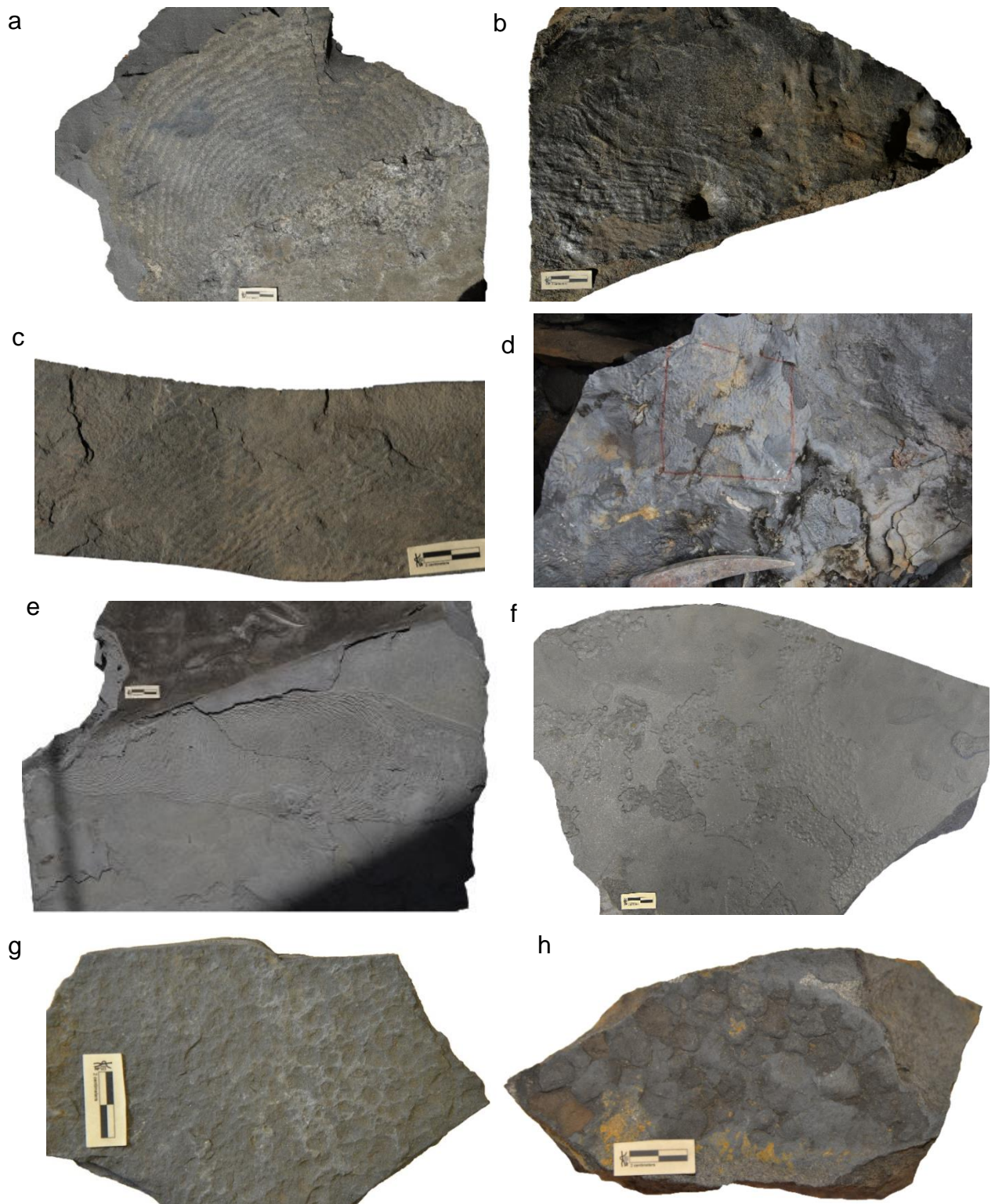
**Fig. S3.** Reflected-light photographs of selected Francevillian microbially induced sedimentary structures. (A) Ring-shaped structures. (B) Wrinkle structures. (C, D) Kinneyia structures. (E) Horizontal mat growth pattern. Oriented structure resulted in numerous small ridges. (F) Domal buildups. (G, H) Elephant-skin textures. Scale bars are 2 cm (for more details see (1)).
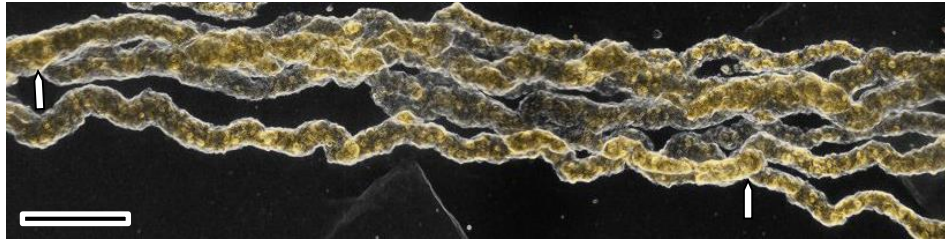
**Fig. S4.** Volume rendering of twinned contorted string-shaped structures with host-rock transparency. Arrows point to braided portion of the **string-shaped structures** (see *SI Appendix,* Video S4). Scale bar is 2 cm.
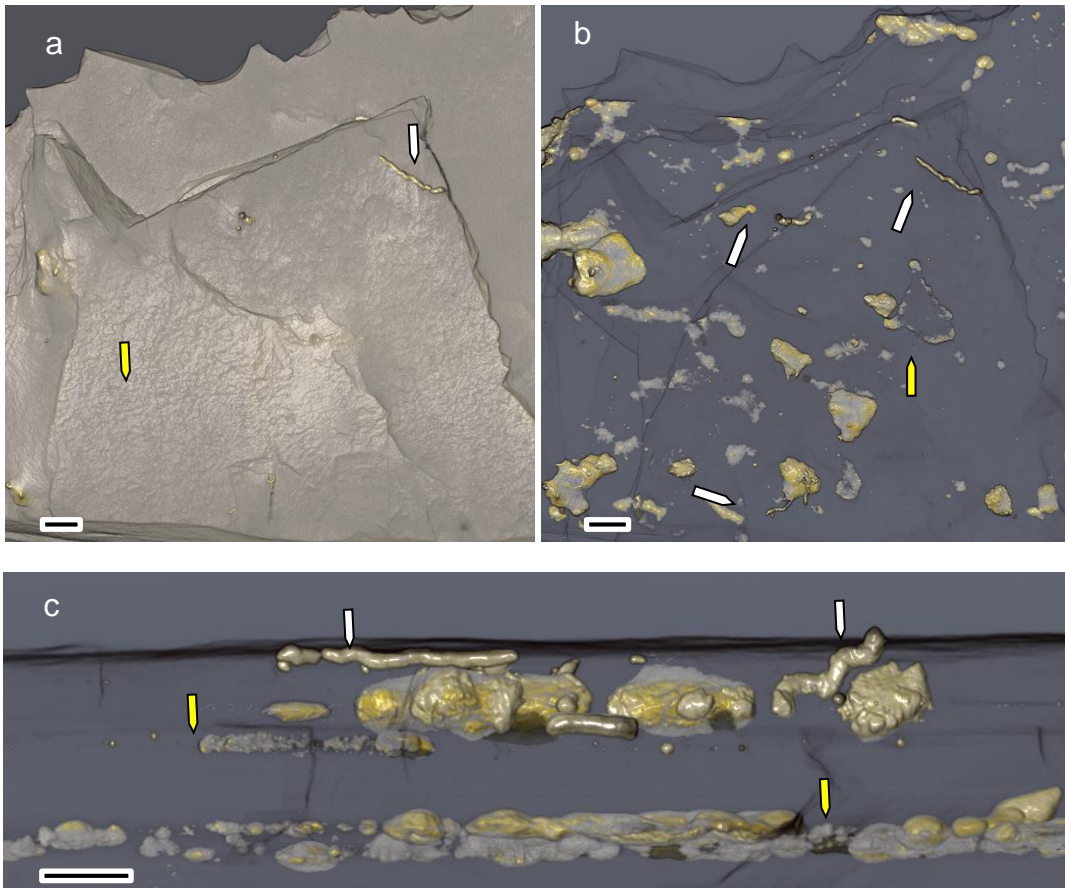


**Fig. S5.** Micro-CT based reconstructions of pyritized string-shaped structures. (A) Volume rendering showing the external surface. (B, C) Volume rendering with host-rock transparency, top surface and lateral views, respectively. White and yellow arrows point to the string-shaped structures and the microbial mat, respectively. Oblique to vertical position of strings is observed at the right side of lateral view. White and yellow arrows point to string-shaped specimens and microbial mats, respectively. Scale bars are 2 cm.
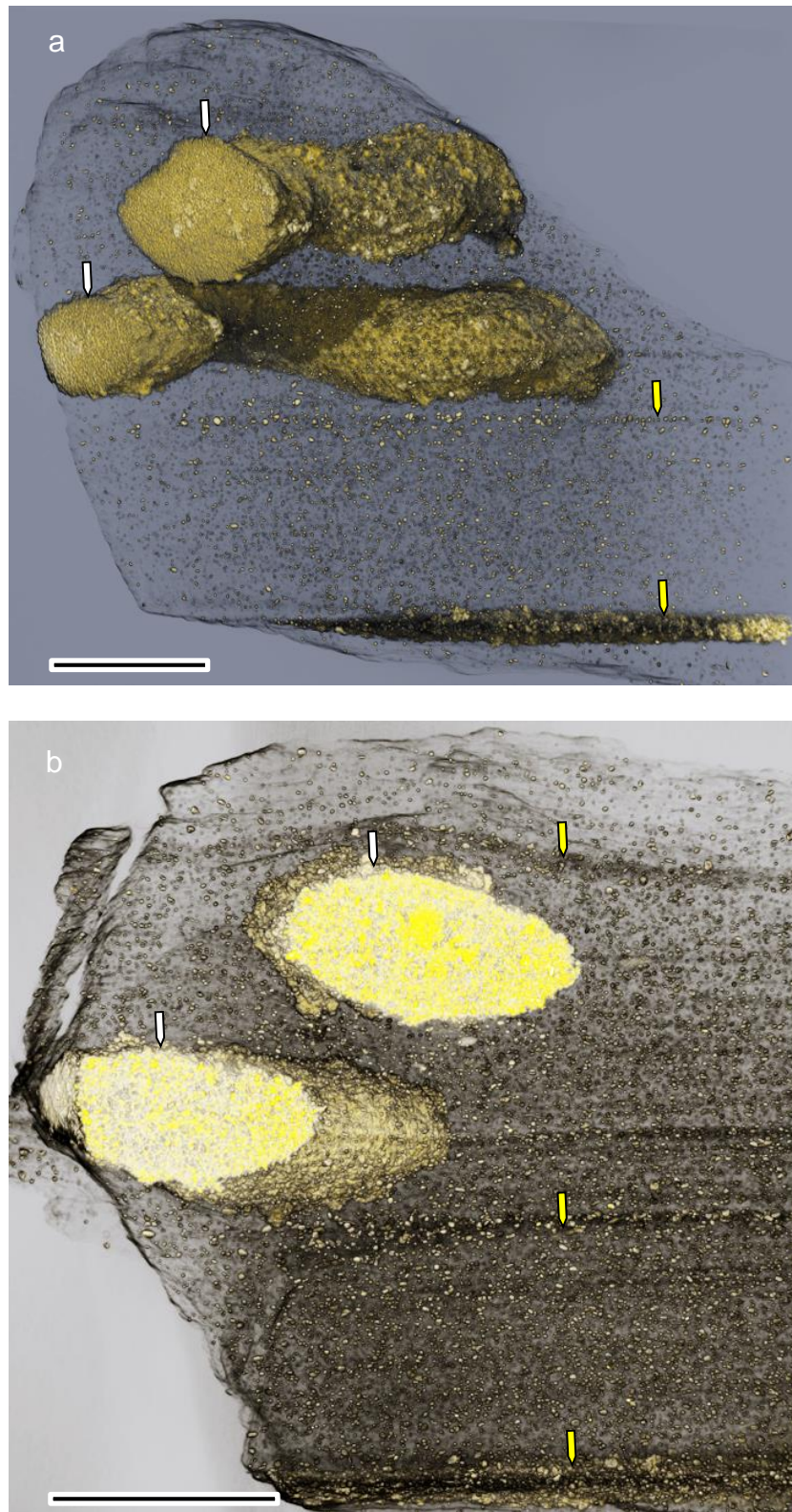
**Fig. S6.** High-resolution micro-CT based reconstruction of a sample portion showing sinuous string-shaped structures and silty shale laminae. (A, B) Volume rendering with host-rock transparency. (A) Representation of the complete portion scanned. (B) Magnified view of a thick section virtually extracted from A. White and yellow arrows point to the strings and microbial mat, respectively. Scale bars are 0.5 cm.
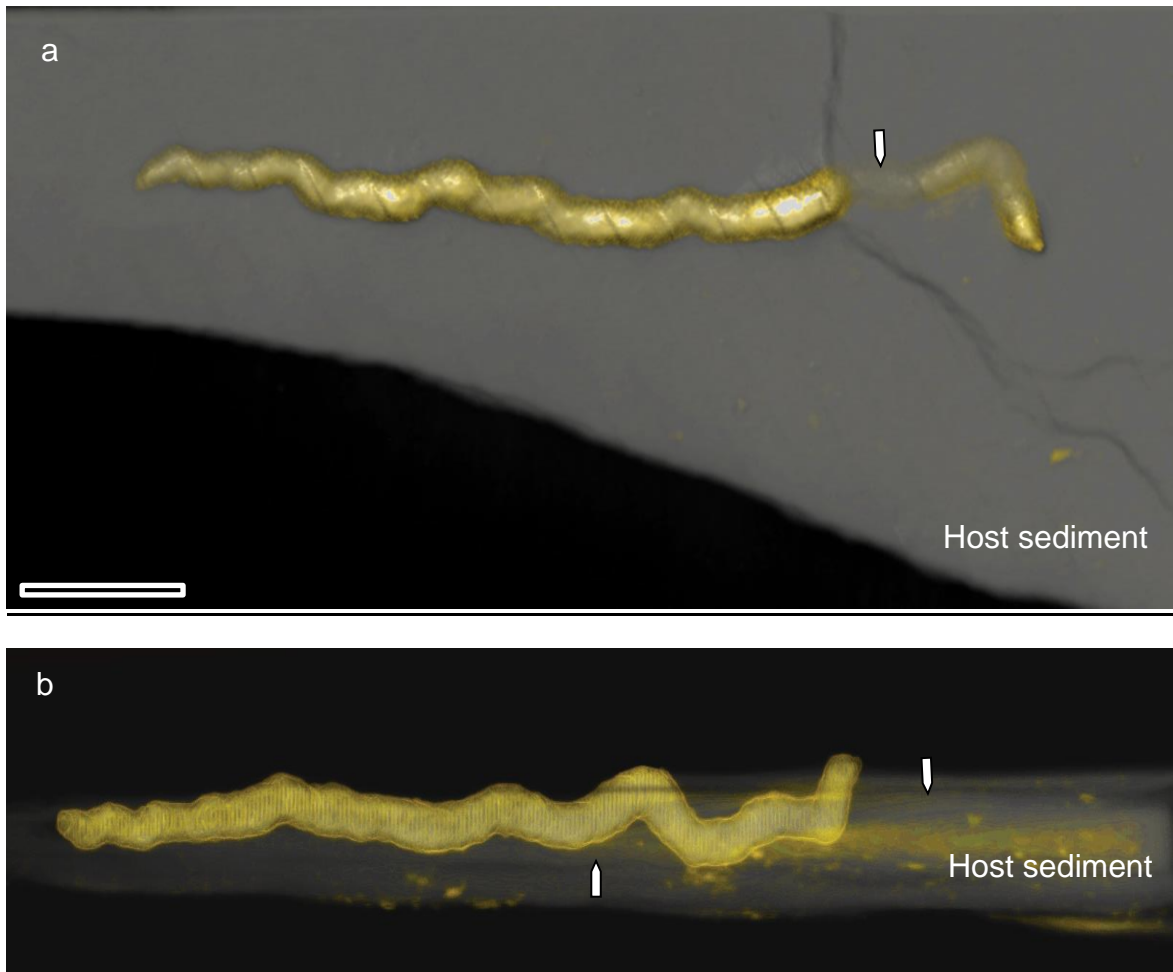
**Fig. S7.** Micro-CT based 3D volume rendering. (A, B) Volume rendering with host-rock transparency showing a string-shaped specimen inside the host rock. (A) Vertical view showing the horizontal sinuosity of the string (white arrow). (B) Lateral view showing the string cutting sediment lamination (white arrows). Scale bars 1 cm.
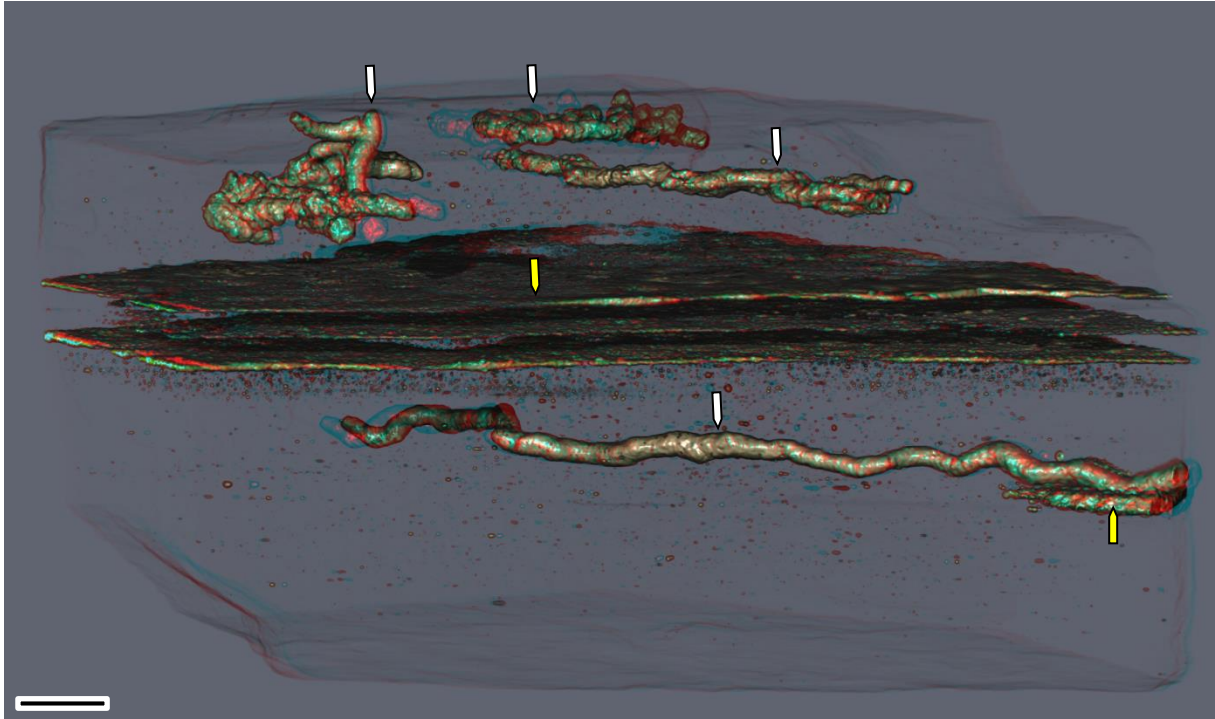
**Fig. S8.** Micro-CT based 3D volume rendering with a stereoscopic 3D effect. Please use red-cyan glasses to reveal the 3D distribution, organization, and relationship between string-shaped structures and host-rock in transparency. White and yellow arrows point to string-shaped structures and microbial mats, respectively (sample shown in Fig. 2D-H). Oblique to vertical position of string-shaped structure is shown at the top-left side. Scale bars are 2 cm.

**a**
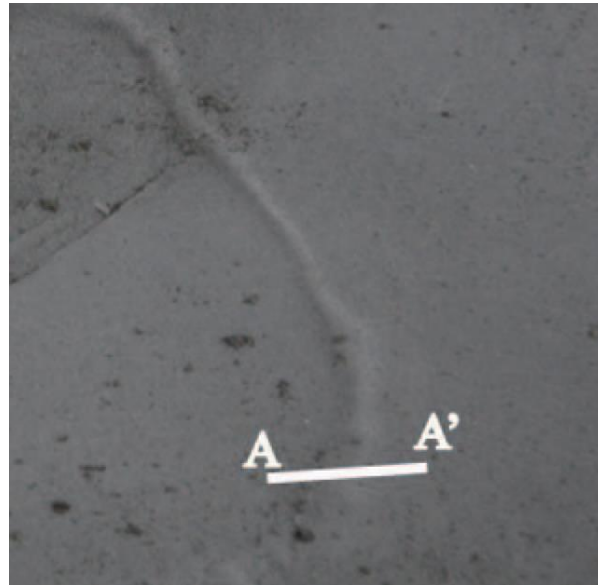


**b**
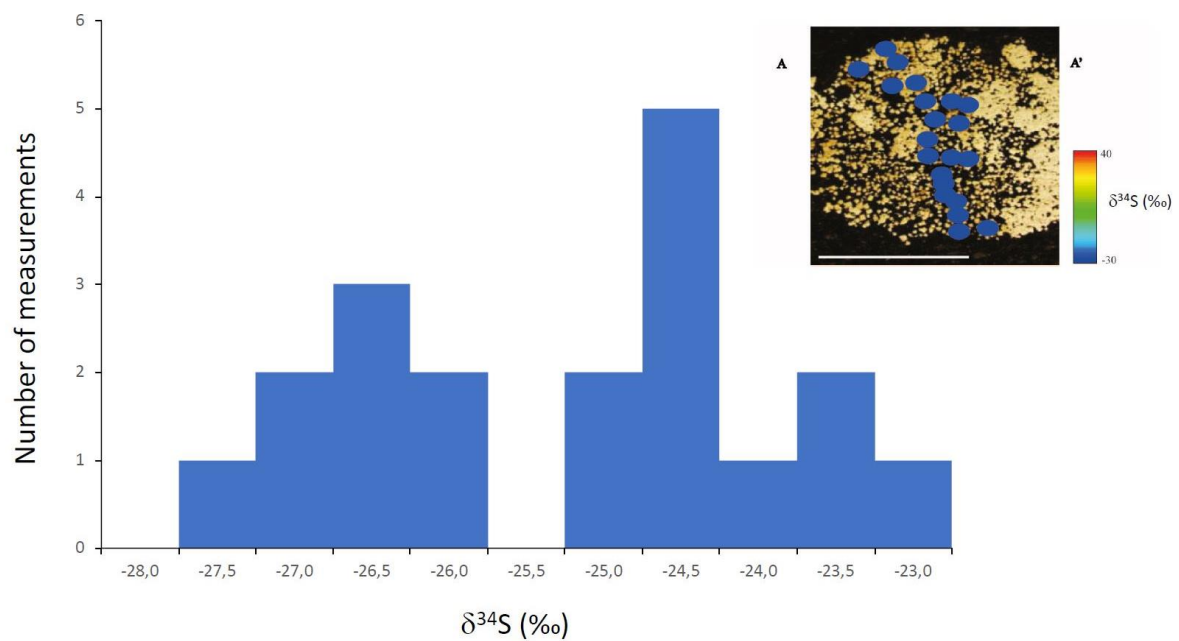


**Fig. S9.** Sulphur-isotope data ($\delta^{34}$S) for pyritized specimen. (A) Section A-A' through the specimen. (B) Corresponding histogram of $\delta^{34}$S values through A-A' (data are from Table S1). Distribution of S isotope values on the maps was rendered following a colour scale increasing from dark blue to red. Scale bars are 0.5 cm.
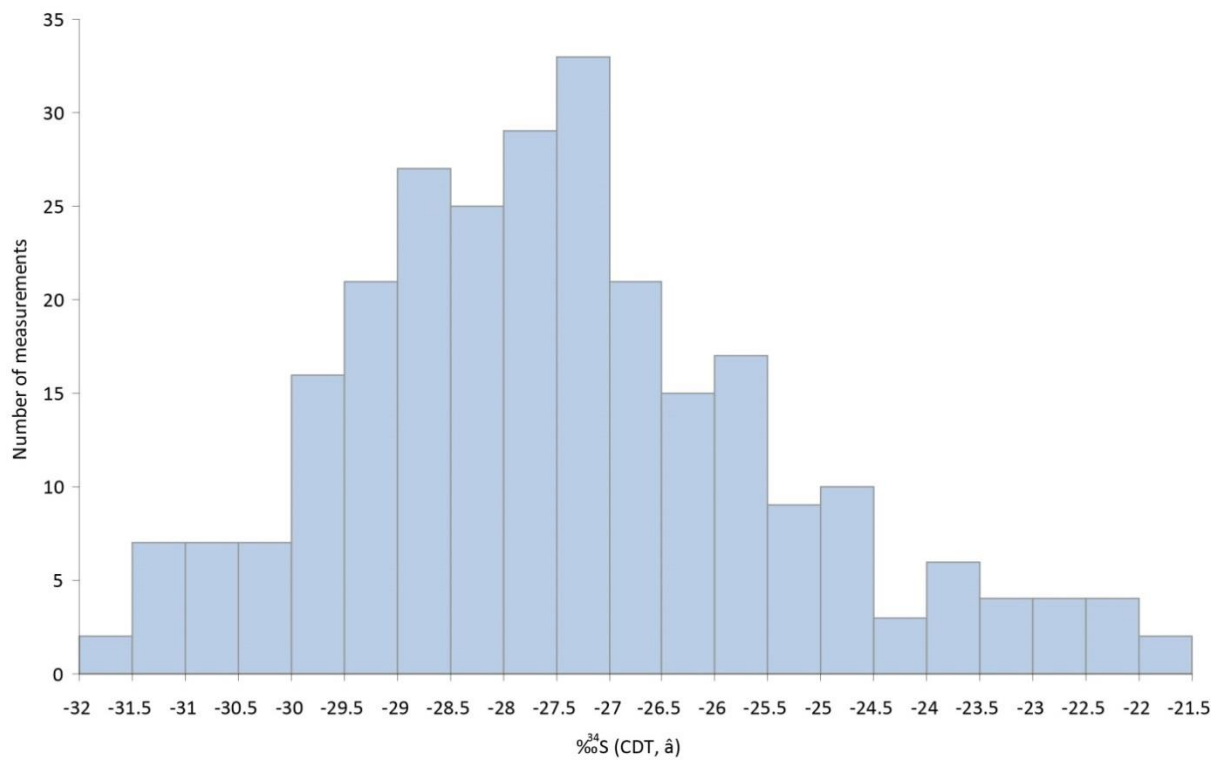
**Fig. S10.** Synthesis of results of $\delta^{34}$S analysis performed by secondary ion mass-spectrometry (SIMS) on selected specimens. Isotope pattern is consistent with the growth of pyrite during early diagenesis.
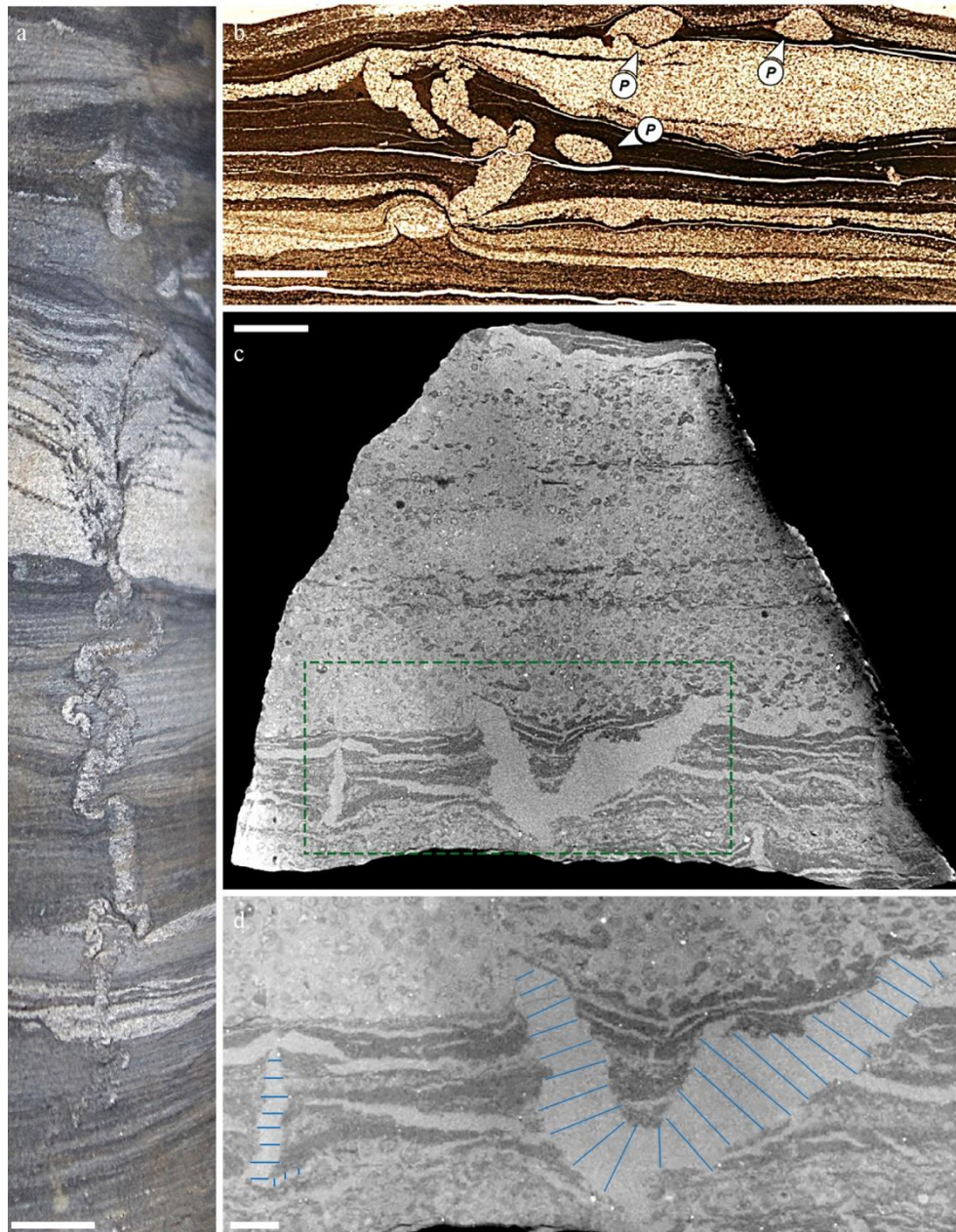
**Fig. S11.** Vertically oriented photograph (A), thin section micrograph (B) and micro-CT scan (C, D) of syneresis cracks. (A) V-shaped, ptygmatically folded vertical cracks filled with silt in black shale layers from the Paleoproterozoic FB1 Member, Gabon. (B) Cracks filled with silt or sand derived from the overlying beds and undeformed bioturbation trace fossils such as *Planolites* 'P' in mudstone beds from the Ordovician Beach Formation of Bell Island. Modified after photo published in (34). (C) Vertical, oblique and horizontal cracks tapering upward and downward in carbonate mudstone beds from the Archean Monteville Formation, South Africa. Dashed green box denotes area magnified in d. Modified after micro-CT scan published in (35). (D) magnified view of box area in C. Blue lines highlight the highly variable size of oblique, vertical and horizontal syneresis cracks. Scale bars are 5 mm (A-C) and 2 mm (D). See *SI Appendix*, Table S2 for comparison of cracks, bioturbation trace fossils, and trails.
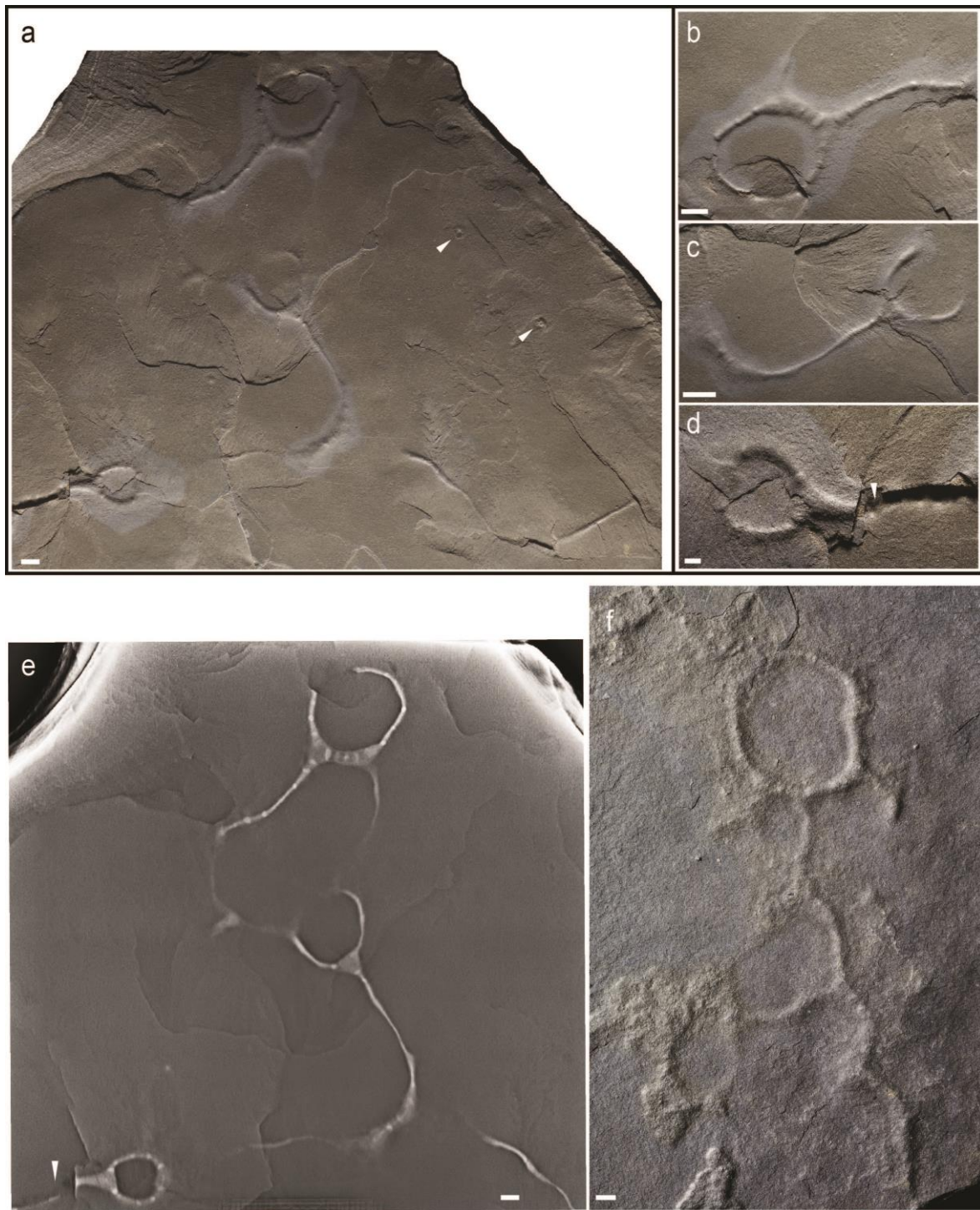
**Fig. S12.** Reflected-light photographs of pyritized string-shaped structures from the Francevillian Series, Gabon. (A-D) Slab displaying structures composed of two connected units. Detailed views of each specimen are in B-D. Structures presented by irregular, connected cercal parts that are elongated and half circular to circular. Small globules of pyrite are distributed at equal spacing along structures. (E) Micro-CT-based reconstruction of structures displayed in A showing external surface volume rendering. White arrows show the ring-shaped structures (14). (F) Slab displaying structures with irregular cercal parts, connected to each other. Scale bars are 1 cm.

**Supplementary Videos**

**Captions for the supplementary videos. 3D animation videos corresponding to five specimens. Please use the links to upload the videos.**

**Video S1** (3D animation). Microtomographic reconstruction showing inner structures through transparency and sequence of virtual cross sections through the specimens. This 3D animation focuses on the horizontally and vertically oriented string-shaped structures and on their relationship with host rock and bacterial mats.

**Video S2** (3D animation). Microtomographic reconstruction showing inner structures through transparency and sequence of virtual cross sections through specimens. This 3D animation focuses on the horizontally and vertically oriented string-shaped structures, their relationship with host rock and bacterial mats.

**Video S3** (3D animation). Microtomographic reconstruction showing inner structures through transparency and sequence of virtual cross sections through specimens. This 3D animation focuses on the varying width of the string-shaped structures and on their position with respect to the bacterial mat.

**Video S4** (3D animation). Microtomographic reconstruction showing inner structures through transparency and sequence of virtual cross sections through specimens. This 3D animation focuses on the twinned string-shaped structures parting from each other and on their varying width.

**Video S5** (3D animation). Microtomographic reconstruction showing inner structures through transparency and sequence of virtual cross sections through specimens. This 3D animation focuses on pyritized string-shaped structures forming a network of interconnecting rings.

**Table S1.** Sulphur isotope values ($\delta^{34}$S) for 15 specimens (n=354 data) from the FB2 Formation. All data were obtained with SIMS.

| Samples | d$^{34}$S (‰) | error (1σ) | | Samples | d$^{34}$S (‰) | error (1σ) |
|---|---|---|---|---|---|---|
| **G-FB2-s12-1** | | | | **G-FB2-s12-2** | | |
| | -29.87 | 0.26 | | | -27.01 | 0.28 |
| | -30.28 | 0.28 | | | -27.46 | 0.27 |
| | -28.56 | 0.26 | | | -25.08 | 0.28 |
| | -29.16 | 0.28 | | | -27.63 | 0.27 |
| | -29.41 | 0.3 | | | -27.46 | 0.28 |
| | -30.93 | 0.29 | | | -27.65 | 0.29 |
| | -29.24 | 0.28 | | | -25.59 | 0.28 |
| | -29.3 | 0.28 | | | -27.7 | 0.28 |
| | -28.31 | 0.28 | | | -27.98 | 0.28 |
| | -30.5 | 0.28 | | | -27.86 | 0.28 |
| | -28.76 | 0.3 | | | -26.46 | 0.28 |
| | -30.26 | 0.29 | | | -27.26 | 0.28 |
| | -29.71 | 0.29 | | | -29.61 | 0.27 |
| | -28.68 | 0.28 | | | -26.73 | 0.27 |
| | -29.18 | 0.29 | | | -25.77 | 0.28 |
| | -29.15 | 0.31 | | | -27.05 | 0.28 |
| | -27.25 | 0.29 | | | -28.02 | 0.29 |
| | -29.07 | 0.28 | | | -27.72 | 0.28 |
| | -28.5 | 0.28 | | | -26.86 | 0.28 |
| | -29.92 | 0.28 | | | -26.71 | 0.27 |
| | -27.24 | 0.28 | | | | |
| | -31.1 | 0.29 | | **G-FB2-s13-4** | | |
| | -29.77 | 0.27 | | | -26.93 | 0.13 |
| | | | | | -28.28 | 0.13 |
| **G-FB2-s13-3** | | | | | -27.53 | 0.13 |
| | -27.1 | 0.12 | | | -27.34 | 0.14 |
| | -26.46 | 0.14 | | | -28.53 | 0.14 |
| | -27.67 | 0.14 | | | -27.98 | 0.12 |
| | -26.52 | 0.13 | | | -27.71 | 0.12 |
| | -25.91 | 0.13 | | | -27.58 | 0.12 |
| | -25.98 | 0.16 | | | -27.52 | 0.13 |
| | -28.55 | 0.15 | | | -31.18 | 0.13 |
| | -25.55 | 0.13 | | | | |
| | -26.51 | 0.13 | | **G-FB2-s14-6** | | |
| | -27.16 | 0.13 | | | -27.19 | 0.14 |
| | -27.05 | 0.11 | | | -28.7 | 0.13 |
| | -27.08 | 0.12 | | | -26.75 | 0.15 |
| | -25.95 | 0.14 | | | -28.36 | 0.14 |

| | | | | | |
|---|---|---|---|---|---|
| | -25.73 | 0.14 | | | -27.95 | 0.13 |
| | -26.92 | 0.15 | | | -28.38 | 0.12 |
| | -28.19 | 0.13 | | | -28.98 | 0.12 |
| | -27.76 | 0.12 | | | -28.14 | 0.13 |
| | | | | | -28.34 | 0.13 |
| **G-FB2-s14-5** | | | | | -27.51 | 0.14 |
| | -30.32 | 0.15 | | | | |
| | -30.51 | 0.14 | | **G-FB2-s14-7** | | |
| | -29.32 | 0.14 | | | -27.42 | 0.27 |
| | -28.78 | 0.13 | | | -28.37 | 0.27 |
| | -28.76 | 0.14 | | | -31.07 | 0.29 |
| | -29.11 | 0.14 | | | -29.83 | 0.29 |
| | -28.66 | 0.13 | | | -22.22 | 0.28 |
| | -29.19 | 0.14 | | | -31.23 | 0.29 |
| | -28.56 | 0.13 | | | -29.33 | 0.27 |
| | -28.91 | 0.13 | | | -29.51 | 0.28 |
| | -28.41 | 0.14 | | | -30.27 | 0.28 |
| | -28.38 | 0.14 | | | -30.66 | 0.28 |
| | -28.94 | 0.13 | | | -29.26 | 0.27 |
| | -28.75 | 0.13 | | | -25.95 | 0.27 |
| | -28 | 0.13 | | | -27.75 | 0.27 |
| | | | | | -27.5 | 0.28 |
| **G-FB2-s14-8** | | | | | -30.05 | 0.27 |
| | -31.61 | 0.29 | | | | |
| | -27.86 | 0.25 | | **G-FB2-s15-9** | | |
| | -23.83 | 0.24 | | | -28.85 | 0.26 |
| | -30.73 | 0.28 | | | -31.06 | 0.3 |
| | -30.82 | 0.28 | | | -29.97 | 0.26 |
| | -24.97 | 0.24 | | | -29.26 | 0.28 |
| | -30.07 | 0.26 | | | -28.44 | 0.26 |
| | -26.45 | 0.24 | | | -29.72 | 0.26 |
| | -29.25 | 0.27 | | | -28.33 | 0.27 |
| | -30.34 | 0.29 | | | -28.58 | 0.27 |
| | | | | | -31.83 | 0.3 |
| **G-FB2-s15-10** | | | | | -26.52 | 0.26 |
| | -22.54 | 0.17 | | | -25.95 | 0.23 |
| | -28.45 | 0.19 | | | -27.31 | 0.27 |
| | -25.51 | 0.21 | | | -28.63 | 0.25 |
| | -28.32 | 0.16 | | | -27.98 | 0.26 |
| | -22.94 | 0.18 | | | -28.1 | 0.27 |
| | -29.44 | 0.19 | | | -29.24 | 0.27 |
| | -28.82 | 0.17 | | | -27.19 | 0.26 |
| | -28.85 | 0.17 | | | -28.45 | 0.28 |

| | | | | | | |
|---|---|---|---|---|---|---|
| | -22.46 | 0.2 | | | -29.11 | 0.24 |
| | -25.18 | 0.17 | | | -20.56 | 0.28 |
| | -29.1 | 0.17 | | | -29.98 | 0.26 |
| | -28.89 | 0.16 | | | -30.72 | 0.3 |
| | -22.65 | 0.19 | | | -28.11 | 0.27 |
| | -22.97 | 0.16 | | | -28.19 | 0.27 |
| | -22.35 | 0.17 | | | -28.79 | 0.27 |
| | -29.75 | 0.19 | | | -29.73 | 0.28 |
| | -28.95 | 0.2 | | | -28.8 | 0.28 |
| | | | | | -31.21 | 0.27 |
| **G-FB2-s15-11** | | | | | | |
| | -27.45 | 0.19 | | **G-FB2-s15-12** | | |
| | -27.83 | 0.24 | | | -26.4 | 0.17 |
| | -27.98 | 0.36 | | | -26.63 | 0.19 |
| | -28.15 | 0.2 | | | -27.37 | 0.21 |
| | -27.87 | 0.21 | | | -25.48 | 0.16 |
| | -27.16 | 0.19 | | | -24.77 | 0.18 |
| | -27.45 | 0.22 | | | -24.63 | 0.19 |
| | -26.65 | 0.22 | | | -25.44 | 0.17 |
| | -27.98 | 0.17 | | | -24.29 | 0.17 |
| | -27.99 | 0.2 | | | -23.22 | 0.2 |
| | -27.36 | 0.18 | | | -23.82 | 0.17 |
| | -28.51 | 0.18 | | | -24.51 | 0.17 |
| | -27.68 | 0.17 | | | -24.53 | 0.16 |
| | -27.47 | 0.19 | | | -23.63 | 0.19 |
| | -28.98 | 0.17 | | | -24.88 | 0.16 |
| | -29.84 | 0.17 | | | -26.85 | 0.17 |
| | -28.42 | 0.16 | | | -26.48 | 0.19 |
| | -29.07 | 0.17 | | | -26.85 | 0.2 |
| | | | | | -27.28 | 0.16 |
| | | | | | -27.7 | 0.18 |
| | | | | | | |
| **G-FB2-s16-13** | | | | **G-FB2-s16-14** | | |
| | -23.45 | 0.36 | | | -31.05 | 0.34 |
| | -24.9 | 0.36 | | | -29.18 | 0.39 |
| | -26.13 | 0.42 | | | -29.07 | 0.35 |
| | -25.58 | 0.37 | | | -29.89 | 0.35 |
| | -23.29 | 0.36 | | | -25.73 | 0.39 |
| | -23.62 | 0.35 | | | -26.19 | 0.4 |
| | -23.03 | 0.37 | | | -29.8 | 0.28 |
| | -26.12 | 0.36 | | | -25.94 | 0.34 |
| | -21.6 | 0.35 | | | -25.11 | 0.38 |
| | -25.6 | 0.37 | | | -25.1 | 0.35 |

| | | | | | | |
|---|---|---|---|---|---|---|
| | -24.7 | 0.36 | | | -26.27 | 0.35 |
| | -26.02 | 0.36 | | | -24.53 | 0.34 |
| | -27.11 | 0.36 | | | -23.99 | 0.35 |
| | -26.66 | 0.36 | | | -23.75 | 0.34 |
| | -26.14 | 0.36 | | | -25.03 | 0.35 |
| | -28.1 | 0.36 | | | -26.46 | 0.36 |
| | -22.03 | 0.36 | | | -25.05 | 0.35 |
| | -24.53 | 0.36 | | | -28.77 | 0.33 |
| | -24.28 | 0.36 | | | -29.74 | 0.31 |
| | -27.3 | 0.36 | | | | |
| | -25.89 | 0.36 | | | | |
| | -24.07 | 0.35 | | | | |
| | -26.14 | 0.37 | | | | |
| | | | | | | |
| **G-FB2-s16-15** | | | | | | |
| | -27.38 | 0.18 | | | | |
| | -27.67 | 0.17 | | | | |
| | -26.98 | 0.17 | | | | |
| | -27.78 | 0.15 | | | | |
| | -27.17 | 0.19 | | | | |
| | -27.11 | 0.18 | | | | |
| | -26.05 | 0.15 | | | | |
| | -26.66 | 0.17 | | | | |
| | -25.66 | 0.13 | | | | |
| | -27.88 | 0.18 | | | | |
| | -26.57 | 0.21 | | | | |
| | -27.43 | 0.16 | | | | |
| | -28.16 | 0.23 | | | | |
| | -28.09 | 0.18 | | | | |
| | -27.42 | 0.16 | | | | |
| | -27.42 | 0.14 | | | | |
| | -27.34 | 0.16 | | | | |
| | -26.6 | 0.16 | | | | |
| | -27.36 | 0.19 | | | | |
| | -26.64 | 0.15 | | | | |
| | -25.64 | 0.16 | | | | |
| | -26.88 | 0.15 | | | | |

**Table S2:** Comparison between cracks, bioturbations trace fossils, and trails.

| References | Age / Stratigraphy | | Shape (plan view) | Measurments (in plan view) | Shape (vertical cross-section view) | Size (in vertical cross-section view) | Host lithology | Infill | Connection with an overlying or underlying bed | Authigenic mineralization | Textural fabric of host laminae |
|---|---|---|---|---|---|---|---|---|---|---|---|
| McMahon *et al.*, 2017 | Quaternary to Archean | C: | Aligned or breaching spindles; partially or fully connected branches and polygons; curlicue cracks; sinuous ripple-trough cracks | Wide range | Upward- and downward-tapering, ptygmatically folded; horizontal | Highly variable | Heterolithic facies | Sand; silt; mud; calcite; dolomite | Yes | Yes | Cut and distortion of background laminae |
| Harazim *et al.*, 2013 | Early Ordovician | C: | Straight to curved doubly-tapering; irregular, poorly organized network | 0.1-0.5 cm wide; 10-20 cm long | Highly contorted; ptygmatically folded | Highly variable | Shale | Sand | Yes | Not reported | Crossed-cutting by cracks |
| | | B: | *Planolites** | 0.4 cm wide; 2.6 cm long | Elliptic to slightly elongated | Constant | | Sand | No | | Bent and intersected by burrows |
| Pratt, 1998 | Mesoproterozoic | C: | Sub-parallel lenticular; sinusoidal; polygonal | 0.1-1 cm wide; 1-30 cm long | Parallel-sided, lenticular; V-shaped tapering upward and downward; ptygmatic; horizontal | Highly variable | Sandstone; siltsone; mudstone | Sand; silt | Yes | Not reported | Folded and broken |
| This study | Paleoproterozoic (FB2 Formation) | T: | **String-like structures** | 0.1-0.6 cm wide; up to 17 cm long | **Elliptic to slightly elongated** | **Constant** | Black shales | **Pyrite** | **No** | Yes | Bent and intersected by pyrite strings |
| | (FB1 Formation) | C: | Unknown | Unknown | V-shaped tapering upward and downward; ptygmatically folded | Highly variable | Black shales | Silt | Yes | Unknown | Cut by the crack |

C: Cracks;    B: Bioturbations;    T: Trails;    * Used for comparison.

**References for SI reference citations**

1. Aubineau J, et al. (2018) Unusual microbial mat-related structural diversity 2.1 billion years ago and implications for the Francevillian biota. *Geobiology* 16(5):476–497.

2. Gerdes G, et al. (1993) Contribution of microbial mats to sedimentary surface structures. *Facies* 29(1):61.

3. Gerdes G, Krumbein W., Reineck H-E (1994) Microbial mats as architects of sedimentary surface structures. *Biostabilization of Sediments* (Bibliotheks- und Informationsystem der Carl von Ossietzky Universität Oldenberg, Oldenberg), pp 165–182.

4. Hagadorn JW, Bottjer DJ (1997) Wrinkle structures: Microbially mediated sedimentary structures common in subtidal siliciclastic settings at the Proterozoic-Phanerozoic transition. *Geology* 25(11):1047–1050.

5. Hagadorn JW, Bottjer DJ (1999) Restriction of a late Neoproterozoic biotope; suspect-microbial structures and trace fossils at the Vendian-Cambrian transition. *PALAIOS* 14(1):73–85.

6. Pflueger F (1999) Matground structures and redox facies. *PALAIOS* 14(1):25–39.

7. Bouougri E, Porada H (2002) Mat-related sedimentary structures in Neoproterozoic peritidal passive margin deposits of the West African Craton (Anti-Atlas, Morocco). *Sedimentary Geology* 153(3):85–106.

8. Noffke N, Knoll AH, Grotzinger JP (2002) Sedimentary Controls on the Formation and Preservation of Microbial Mats in Siliciclastic Deposits: A Case Study from the Upper Neoproterozoic Nama Group, Namibia. *PALAIOS* 17(6):533–544.

9. Mariotti G, Pruss SB, Perron JT, Bosak T (2014) Microbial shaping of sedimentary wrinkle structures. *Nature Geoscience* 7(10):736–740.

10. Porada H, Bouougri EH (2007) Wrinkle structures—a critical review. *Earth-Science Reviews* 81(3):199–215.

11. Walcott C D (1914) Cambrian geology and palaeontology III No.2 – Precambrian, Algonkian algal flora. *Smithsonian Miscellaneous Collections* 64:77–156.

12. Thomas K, Herminghaus S, Porada H, Goehring L (2013) Formation of Kinneyia via shear-induced instabilities in microbial mats. *Philos Trans A Math Phys Eng Sci* 371(2004):20120362.

13. Lieleg O, Caldara M, Baumgärtel R, Ribbeck K (2011) Mechanical robustness of Pseudomonas aeruginosa biofilms. *Soft Matter* 7(7):3307–3314.

14. El Albani A, et al. (2014) The 2.1 Ga Old Francevillian Biota: Biogenicity, Taphonomy and Biodiversity. *PLOS ONE* 9(6):e99438.

15. Garlick WG (1988) Algal mats, load structures, and synsedimentary sulfides in Revett quartzites of Montana and Idaho. *Economic Geology* 83(6):1259–1278.

16. Schieber J (1999) Microbial mats in terrigenous clastics; the challenge of identification in the rock record. *PALAIOS* 14(1):3–12.

17. Runnegar B N, Fedonkin M A (1992) Proterozoic Metazoan Body Fossils. *The Proterozoic Biosphere: A Multidisciplinary Study* (Cambridge University Press, Cambridge), pp 369–388.

18. Gerdes G, Klenke T, Noffke N (2000) Microbial signatures in peritidal siliciclastic sediments: a catalogue. *Sedimentology* 47(2):279–308.

19. Shepard RN, Sumner DY (2010) Undirected motility of filamentous cyanobacteria produces reticulate mats. *Geobiology* 8(3):179–190.

20. McMahon S, van Smeerdijk Hood A, McIlroy D (2016) The origin and occurrence of subaqueous sedimentary cracks. *Geological Society, London, Special Publications* 448. doi:10.1144/SP448.15.

21. Pratt BR (1998) Syneresis cracks: subaqueous shrinkage in argillaceous sediments caused by earthquake-induced dewatering. *Sedimentary Geology* 117(1):1–10.

22. Pratt BR (1998) Syneresis cracks: subaqueous shrinkage in argillaceous sediments caused by earthquake-induced dewatering. *Sedimentary Geology* 117(1):1–10.

23. Leach DL, et al. (2005) Sediment-hosted lead-zinc deposits; a global perspective. *Economic Geology; One Hundredth Anniversary Volume, 1905-2005*, eds Hedenquist JWT John FH Goldfarb, Richard J Richards, Jeremy P, Thompson JFH, Goldfarb RJ (Society of Economic Geologists), pp 561–607.

24. Magnall JM, et al. (2016) Open system sulphate reduction in a diagenetic environment – Isotopic analysis of barite ($\delta$34S and $\delta$18O) and pyrite ($\delta$34S) from the Tom and Jason Late Devonian Zn–Pb–Ba deposits, Selwyn Basin, Canada. *Geochimica et Cosmochimica Acta* 180:146–163.

25. Weber F, Gauthier-Lafaye F, Whitechurch H, Ulrich M, El Albani A (2016) The 2-Ga Eburnean Orogeny in Gabon and the opening of the Francevillian intracratonic basins: A review. *Comptes Rendus Geoscience* 348(8):572–586.

26. Lyons TW, Gellatly AM, McGoldrick PJ, Kah LC (2006) Proterozoic sedimentary exhalative (SEDEX) deposits and links to evolving global ocean chemistry. *Geological Society of America Memoirs* 198:169–184.

27. Knott R, Fouquet Y, Honnorez J, Petersen S, Bohn M (1998) Petrology of hydrothermal mineralization: a vertical section through the TAG mound. *Proc. ODP, Sci. Results, 158*, eds Herzig PM, Humphris SE, Miller DJ, Zierenberg RA, pp 5–26.

28. Georgieva MN, Little CTS, Ball AD, Glover AG (2015) Mineralization of Alvinella polychaete tubes at hydrothermal vents. *Geobiology* 13(2):152–169.

29. Peckmann J, et al. (2001) Methane-derived carbonates and authigenic pyrite from the northwestern Black Sea. *Marine Geology* 177(1–2):129–150.

30. Huang CY, Chien CW, Zhao M, Lizuka Y (2006) Geological study of active cold seeps in the syn-collision accretionary prism Kaoping Slope off SW Taiwan. *Terrestrial Atmospheric and Oceanic Sciences* 17(4):679–702.

31. Mazzini A, et al. (2008) Complex plumbing systems in the near subsurface: Geometries of authigenic carbonates from Dolgovskoy Mound (Black Sea) constrained by analogue experiments. *Marine and Petroleum Geology* 25(6):457–472.

32. El Albani AE, et al. (2010) Large colonial organisms with coordinated growth in oxygenated environments 2.1 Gyr ago. *Nature* 466(7302):100–104.

33. Jensen S (2003) The proterozoic and earliest cambrian trace fossil record; patterns, problems and perspectives. *Integr Comp Biol* 43(1):219–228.

34. Harazim D, et al. (2013) Spatial variability of watermass conditions within the European Epicontinental Seaway during the Early Jurassic (Pliensbachian–Toarcian). *Sedimentology* 60(2):359–390.

35. McMahon S, Hood A van S, McIlroy D (2017) The origin and occurrence of subaqueous sedimentary cracks. *Geological Society, London, Special Publications* 448(1):285–309.